Real-time Observation of sub-100-fs Charge and Energy Transfer Processes in DNA Dinucleotides

Vasilis Petropoulos,[a] Lara Martinez-Fernandez, [b]† Lorenzo Uboldi, [a] Margherita Maiuri, [a] Giulio Cerullo,[a,c]* Evangelos Balanikas[d] and Dimitra Markovitsi[e]**

[a] Dipartimento di Fisica, Politecnico di Milano, Piazza Leonardo da Vinci 32, I-20133 Milano, Italy

[b] Instituto de Química Física Blas Cabrera, Consejo Superior de Investigaciones Científicas. Calle Serrano 119, 28006, Madrid, Spain.

[c] Istituto di Fotonica e Nanotecnologie-CNR, Piazza Leonardo da Vinci 32, I-20133 Milano, Italy

[d] Department of Physical Chemistry, University of Geneva, CH-1211 Geneva-4, Switzerland

[e] Université Paris-Saclay, CNRS, Institut de Chimie Physique, UMR8000, 91405 Orsay, France

Electronic Supplementary Information

1. Temporal resolution of the transient absorption experiments

As described in the main text, the 266-nm UV pump pulses are generated as the second harmonic of a broadband visible NOPA. The pulses are compressed to a 24-fs duration (FWHM) with the aid of a prism pair prior to their comprehensive temporal and spectral characterization by two-dimensional spectral interferometry. Details of the experimental setup can be found in reference 1. The transient absorption (*TA*) signal is recorded as a function of the time delay between the pump pulse and a chirped broadband probe pulse generated as a white light continuum (WLC) in a 3-mm-thick CaF_2 plate. We have previously demonstrated that the chirp of the WLC probe has a minimal effect on the overall "effective" time resolution[2] of the *TA* experiment, provided that broadband detection of the *TA* signal with sufficiently high temporal resolution is adopted, as in our case. Chirp correction on the experimental datasets is performed using a custom-made Matlab code, aligning the sharp cross-phase modulation (XPM) responses to mark the zero-time arrival between the pump and probe pulses.

UV *TA* experiments aiming for high temporal resolution are challenging due to the co-presence of pulse dispersion and XPM, caused by the interaction of the pump pulse with the cuvette front and back glass surfaces, as well as XPM and group velocity mismatch between the pump and probe pulses in the sample. We bypass these problems, as previously demonstrated, by using high concentration solutions in 1-mm-pathlength cuvettes.[3] The high concentrations of the samples (dG, dT, equimolar mixture of dT and dG, and **TG**) are crucial because the *TA* signal is only recorded when there is an overlap of the pump and probe pulses. If the first 200 or 300 μm of the 1-mm cuvette pathlength absorbs almost all the pump light, the total thickness of the sample becomes irrelevant, and only the effective thickness matters. In this case the pump pulse intensity on the cuvette back window, which is 1 mm away from the front window, is low enough that the generated XPM artefact is negligible. The dispersion caused by the entrance front glass window of the cuvette on the pump pulses can be pre-compensated by adjusting the negative dispersion introduced by the prism compressor. Additionally, self-absorption of the probe pulse can be safely excluded, as the ground state absorption of the studied molecules (extending at wavelengths shorter than 300 nm) does not overlap with our probe spectrum (320-650 nm).

To confirm the high temporal resolution of our setup, we performed *TA* experiments on dT under the same conditions used for the **TG** dinucleotide, the results of which are reported in Fig. S1. We observe the immediate rise of the stimulated emission (*SE*) signal from the ππ*T state populated by the pump pulse (Fig. S1a). We can estimate the instrumental response function (IRF) of the setup by the time that the *SE* signal takes to rise from 10% to 90% of its maximum, which is 27 fs. We also observe, superimposed to the *SE* dynamics, an oscillatory signal which is due to impulsively excited coherent molecular vibrations (Figure S1(b)). The oscillatory signal arises from the wave packet motion on the excited state potential energy surface[4]. Performing a Fourier transform on the oscillating residuals (Fig. S1c), we observe peaks at 415 cm^{-1}, 490 cm^{-1} and 750 cm^{-1}. The 750 cm^{-1} peak (which corresponds to a 42-fs oscillation period) is typical of a breathing mode of the aromatic ring, characterized by a large amplitude of the N1C6C5 angle.[5] To experimentally resolve such high-frequency modulation, an IRF significantly shorter than the periods of the observed vibrations is required.

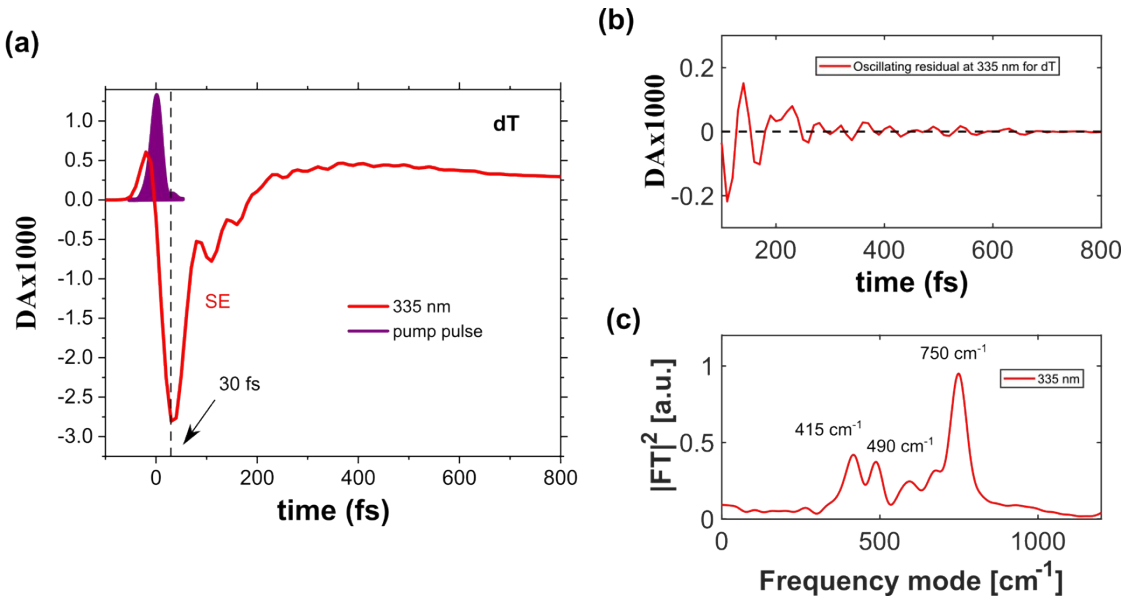

Fig. S1: (a) *TA* dynamics for the monomeric dT at 335 nm probe wavelength. One observes an instantaneous (within the 27-fs IRF) appearance of the *SE*. The *SE* possesses oscillating modulation due to the impulsively generated coherent molecular vibrations. (b) Isolation of the oscillating residual at 335 nm. (c) Fourier Transform (FT) power spectrum obtained after performing FT of the oscillating residuals in order to retrieve the vibrational content of the molecular response.

2. Additional Figures

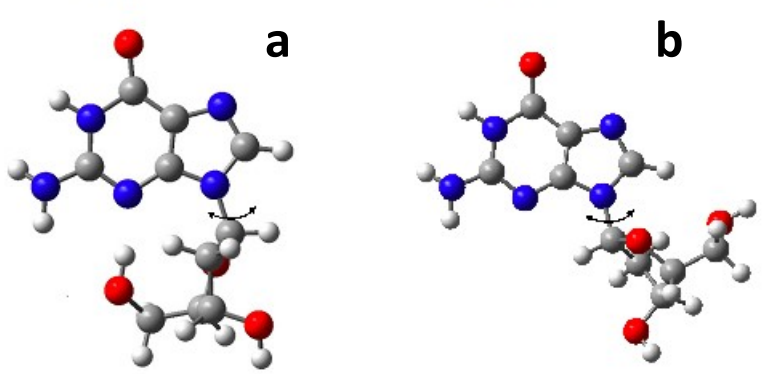

Fig. S2. The *anti-anti* (a) and *anti-syn* (b) conformers of **TG**, encountered, respectively, in B-form duplexes and in G-Quadruplexes; the arrows indicate rotation around the glycosidic bond.

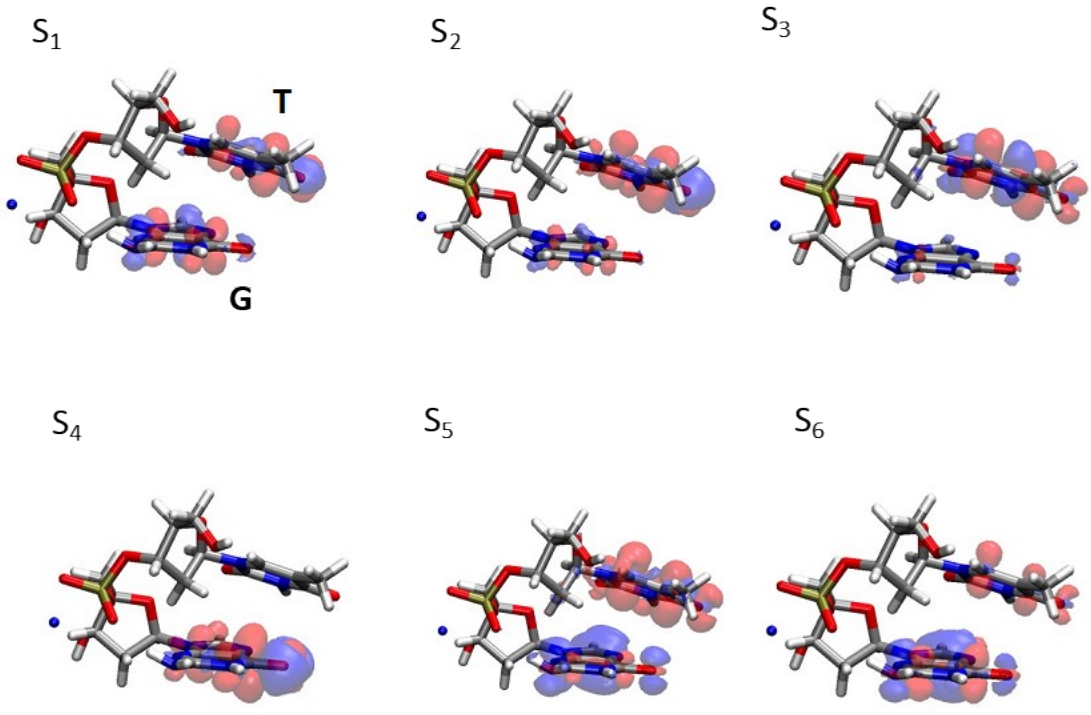

Fig. S3. Excited state-ground state density difference determined for the 6 lowest Franck-Condon states of *anti-syn* **TG**. A decrease in the electronic density is illustrated in blue, while an increase in red.

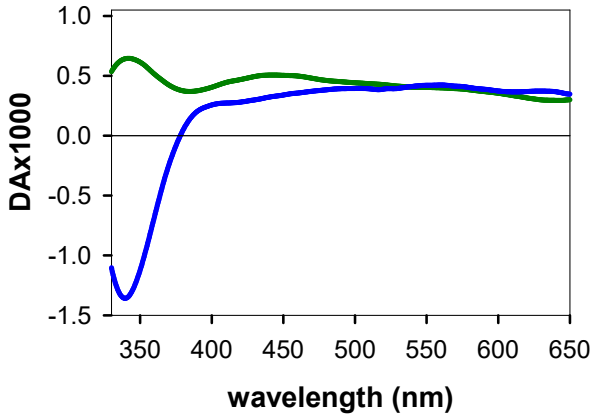

Fig. S4. *TAS* measured for dT (blue) and dG (green) at 50 fs.

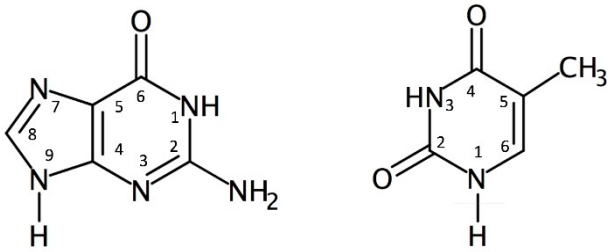

Fig. S5. Atom labelling for the guanine and thymine chromophores.

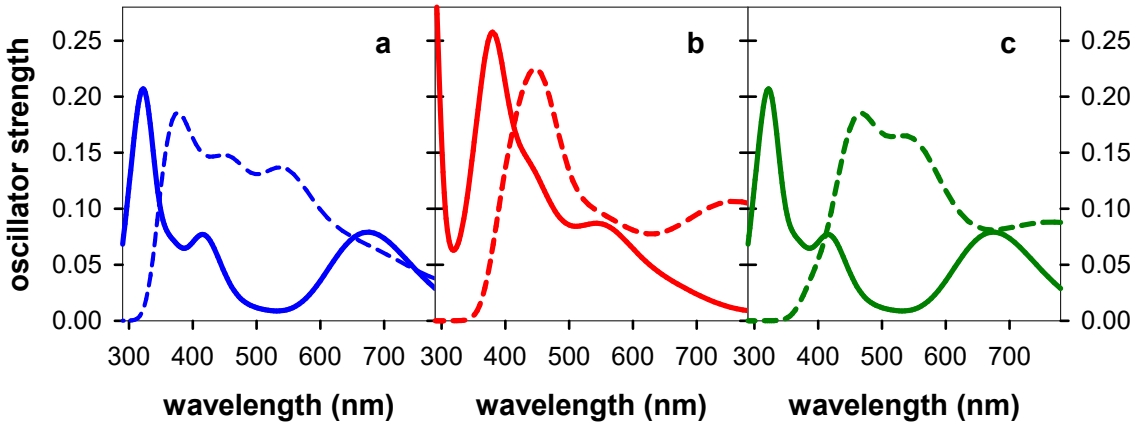

Fig. S6. *TAS* computed for selected Franck-Condon states (dashed lines) and the corresponding minima (solid lines) of *anti-syn* **TG**: $S_3 \rightarrow$ min-ππ*G (a), $S_5 \rightarrow$ min-*CT* (b) and $S_6 \rightarrow$ min-ππ*G (c).

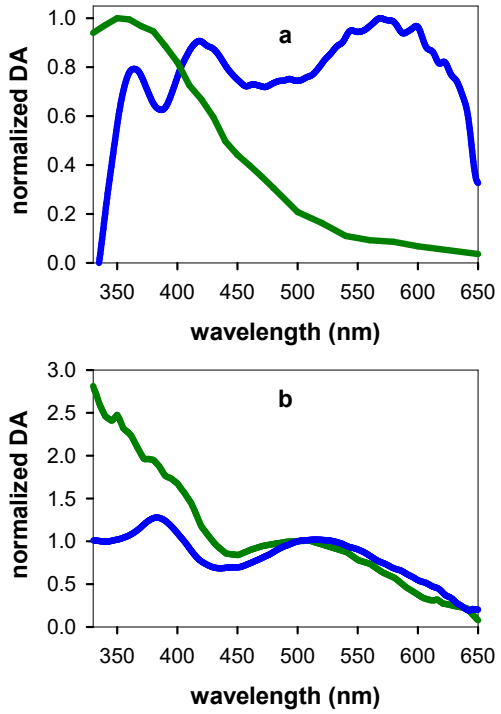

Fig. S7. In blue: *TAS* recorded for **TG** (blue) at 40 ps (a) and 5 ps (b). In green: spectrum of the triplet state determined for thymidine monophosphate by flash photolysis (a);[6] spectrum corresponding to an equimolar mixture of the guanosine radical cation[7] and the thymidine radical anion (b).[8] We note that the anion spectrum, obtained by pulse radiolysis is not accurate in the UV region because this method generates additional transient species.

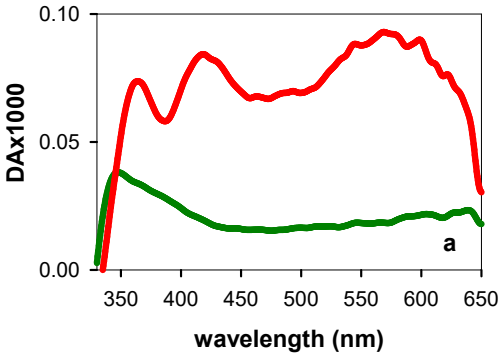

Fig. S8. Comparison of the *TAS* recorded at 40 ps for TG (red) and an equimolar mixture of dT and dG (green).

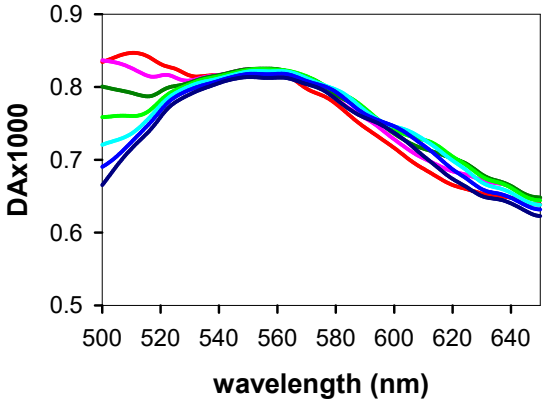

Fig. S9. *TAS* recorded for an equimolar mixture of dT and dG from **40** to **100** fs with 10 fs steps.

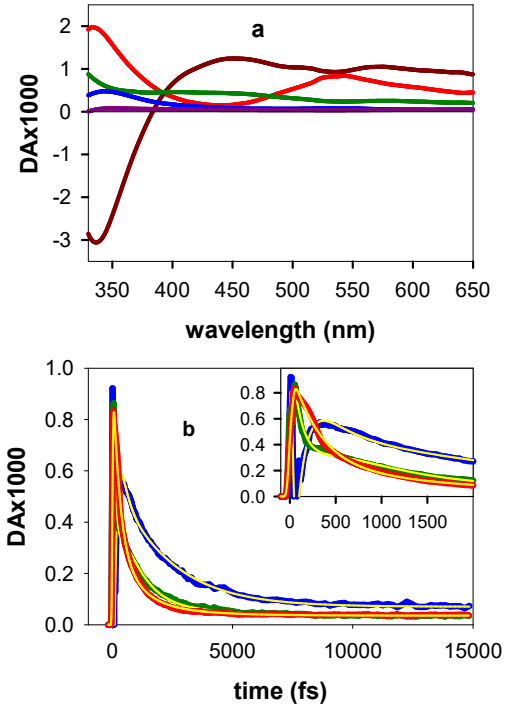

Fig. S10. (a) *EAS* components retrieved from global analysis of the *TA* data for an equimolar mixture of dG and dT and corresponding to time constants of 120 fs (dark red), 250 fs (red), 800 fs (green), 2.1 ps (blue) and 2 ns (violet). (b) Kinetic traces at 365 nm (blue), 445 nm (green) and 520 nm (red) shown together with the fitted functions (yellow).

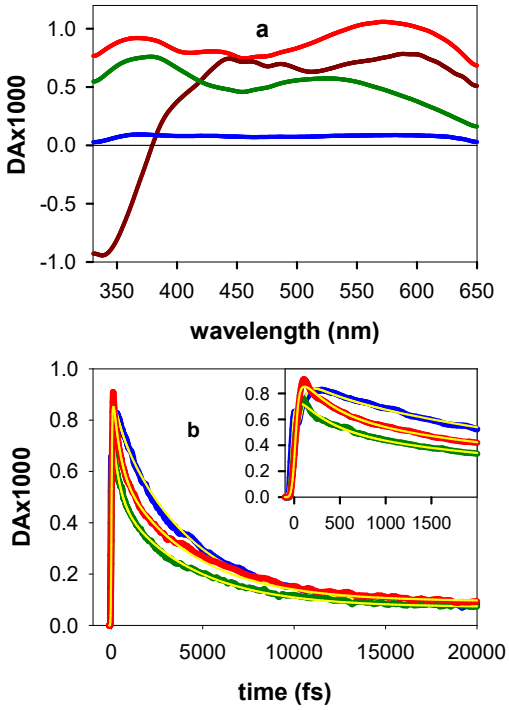

Fig. S11. (a) *EAS* components retrieved from a global analysis of the *TA* data for **TG** and corresponding to time constants of 50 fs (dark red), 380 fs (red), 4.1 ps (green) and 2 ns (blue). (b) Kinetic traces at 365 nm (blue), 445 nm (green) and 520 nm (red) shown together with the fitted functions (yellow).

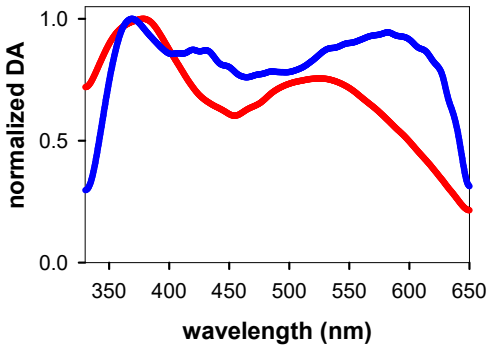

Fig. S12. Normalized *EAS* corresponding to the time constants of 4.1 ps (red) and 2 ns (blue) retrieved from the global analysis performed for the TA data of **TG**.

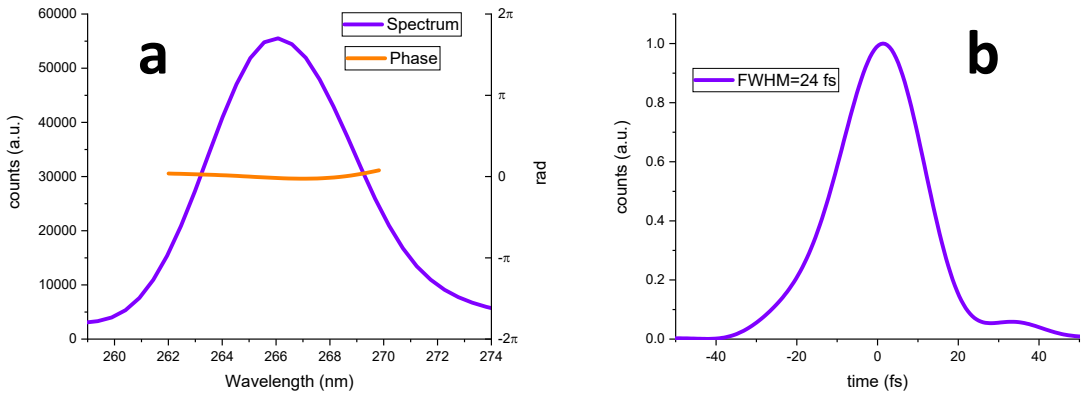

Fig. S13. Full spectral and temporal characterization of the exciting laser pulses.

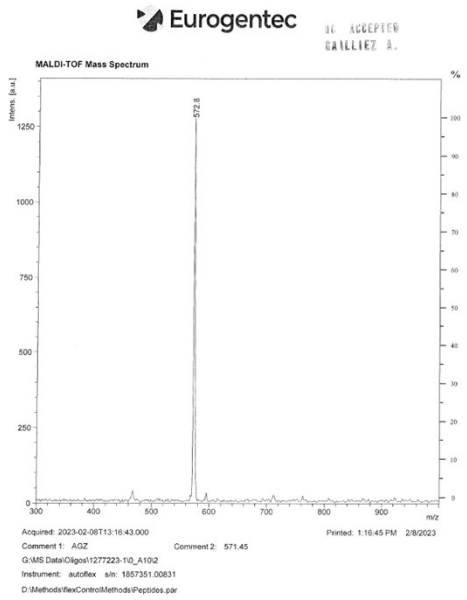

Fig. S14. MALDI-TOF spectrum provided by Eurogentec for **TG**.

Additional Tables

Table S1. Relative energies of the different possible **TG** conformers with respect to the *anti-anti* one, computed at the PCM/M052X/6-31G(d) level of theory.

conformer	ΔE in eV (kcal/mol)	ΔG in eV (kcal/mol)
anti-anti	0.0 (0.0)	0.0 (0.0)
anti-syn	-0.16 (-3.7)	-0.06 (-1.4)
syn-anti	0.11 (2.5)	0.13 (3.1)
syn-syn	0.03 (0.7)	0.11 (2.6)

Table S2. Properties of the Franck-Condon states determined for *anti-anti* **TG** at the PCM/M052X/6-31G(d) level of theory. VAE: vertical absorption energy; f: oscillator strength; δ: charge transfer character.[9]

	character	VAE (eV)	f	δ (a.u.)
S_1	nπ*(T)	5.21	0.001	0.02
S_2	ππ*G(La)	5.29	0.162	0.04
S_3	ππ*T	5.37	0.193	0.02
S_4	nπ*G + ππ*T + *CT*	5.63	0.127	0.20
S_5	nπ*G + ππ*T + *CT*	5.63	0.170	0.23
S_{10}	G→T *CT*	6.78	0.002	0.61

Table S3. Properties of the Franck-Condon states determined for *syn-anti* **TG** at the PCM/M052X/6-31G(d) level of theory. VAE: vertical absorption energy; f: oscillator strength; δ: charge transfer character.

	character	VAE (eV)	f	δ (a.u.)
S_1	nπ*(T)	5.18	0.006	0.02
S_2	ππ*G(La) + *CT*	5.24	0.072	0.37
S_3	ππ*T + *CT*	5.36	0.067	0.13
S_4	ππ*T + *CT*	5.47	0.126	0.35
S_5	nπ*G	5.62	0.001	0.01
S_{10}	G→T *CT*	6.70	0.019	0.57

Table S4. Properties of the Franck-Condon states determined for *syn-syn* **TG** at the PCM/M052X/6-31G(d) level of theory. VAE: vertical absorption energy; f: oscillator strength; δ: charge transfer character.

	character	VAE (eV)	f	δ (a.u.)
S_1	ππ*G(La)	5.19	0.040	0.11
S_2	nπ*(T)	5.23	0.001	0.02
S_3	ππ*T + *CT*	5.38	0.309	0.20
S_4	nπ*G	5.62	0.040	0.02
S_5	ππ* G (Lb)	5.68	0.317	0.08
S_6	G→T *CT*	5.72	0.047	0.52

Table S5. Properties of the minima located on the *PES* of the first excited state determined for *anti-syn* **TG** at the PCM/M052X/6-31G(d) level of theory. ADE: adiabatic (with respect to the S_0 at the FC region) energies; VEE: vertical (with respect to the S_0 at the corresponding minima) emission energies; f: oscillator strengths; initial state optimized and main reaction coordinate.

	ADE (eV)	VEE (eV)	f	initial state	Reaction coordinate
min-ππ*G (La)	4.36	2.06	0.0153	S_1, S_3, S_6	C1-C2-NH2
min-*CT*	4.50	3.23	0.088	S_5	Interbase distance + Ring T
min-nπ*T	4.77	3.91	0.0014	S_2, S_4	C4-O4

Table S6. Properties of the minima located on the *PES* of the first excited state determined for *anti-anti* **TG** at the PCM/M052X/6-31G(d) level of theory. ADE: adiabatic (with respect to the S_0 at the FC region) energies; VEE: vertical (with respect to the S_0 at the corresponding minima) emission energies; f: oscillator strengths; initial state optimized. S_4 arrives directly to a S_1/S_0 degeneracy region.[9] For completeness we have also characterized S_5 that arrives to a CT minimum but being the *anti-syn* **TG** one and requiring a very large rearrangement of the bases.

	ADE (eV)	VEE (eV)	f	initial state
min-ππ*G (La)	4.46	1.98	0.018	S_2
min-ππ*T	4.29	3.27	0.126	S_3, S_{10}
min-nπ*T	4.58	3.80	0.004	S_1

Table S7. Properties of the minima located on the *PES* of the first excited state determined for *syn-anti* **TG** at the PCM/M052X/6-31G(d) level of theory. ADE: adiabatic (with respect to the S_0 at the FC region) energies; VEE: vertical (with respect to the S_0 at the corresponding minima) emission energies; f: oscillator strengths; initial state optimized and main reaction coordinate.

	ADE (eV)	VEE (eV)	f	initial state	Reaction coordinate
min-nπ*G (La)	4.55	1.17	0.003	S_3	C6-O6
min-*CT*	4.31	3.32	0.024	S_2, S_{10}	Interbase distance + Ring T
min-nπ*T	4.76	3.78	0.002	S_1, S_4, S_5	C4-O4

Table S8. Properties of the minima located on the *PES* of the first excited state determined for *syn-syn* **TG** at the PCM/M052X/6-31G(d) level of theory. ADE: adiabatic (with respect to the S_0 at the FC region) energies; VEE: vertical (with respect to the S_0 at the corresponding minima) emission energies; f: oscillator strengths; initial state optimized and main reaction coordinate. S_2 S_4 arrives directly to S_1/S_0 degeneracy regions.

	ADE (eV)	VEE (eV)	f	initial state	Reaction coordinate
min-ππ*G (La)	4.44	2.08	0.0164	S_3	C1-C2-NH2
CI-CT				S_2, S_5 and S_6	Dimerization C5T-C8G
min-nπ*T	4.80	3.90	0.0009	S_1	C4-O4

References

1. R. Borrego-Varillas, A. Oriana, F. Branchi, S. De Silvestri, G. Cerullo and C. Manzoni, Optimized ancillae generation for ultra-broadband two-dimensional spectral-shearing interferometry, *J. Opt. Soc. Am. B* 2015, **32**, 1851-1855.
2. D. Polli, D. Brida, S. Mukamel, G. Lanzani and G. Cerullo, Effective temporal resolution in pump-probe spectroscopy with strongly chirped pulses, *Phys. Rev. A*, 2010, **82**.
3. P. Kabacinski, M. Romanelli, E. Ponkkonen, V. K. Jaiswal, T. Carell, M. Garavelli, G. Cerullo and I. Conti, Unified Description of Ultrafast Excited State Decay Processes in Epigenetic Deoxycytidine Derivatives, *J. Phys. Chem. Lett.*, 2021, **12**, 11070-11077.
4. M. Liebel and P. Kukura, Broad-Band Impulsive Vibrational Spectroscopy of Excited Electronic States in the Time Domain, *J. Phys. Chem. Lett.*, 2013, **4**, 1358-1364.
5. R. Borrego-Varillas, A. Nenov, P. Kabacinski, I. Conti, L. Ganzer, A. Oriana, V. K. Jaiswal, I. Delfino, O. Weingart, C. Manzoni, I. Rivalta, M. Garavelli and G. Cerullo, Tracking excited state decay mechanisms of pyrimidine nucleosides in real time, *Nature Comm.*, 2021, **12**.
6. S. Marguet and D. Markovitsi, Time-resolved study of thymine dimer formation, *J. Am. Chem. Soc.*, 2005, **127**, 5780-5781.
7. L. P. Candeias and S. Steenken, Ionization of purine nucleosides and nucleotides and their components by 193-nm laser photolysis in aqueous solution: model studies for oxidative damage of DNA, *J. Am. Chem. Soc.*, 1992, **114**, 699-704.
8. R. Yamagami, K. Kobayashi and S. Tagawa, Formation of Spectral Intermediate G-C and A-T Anion Complex in Duplex DNA Studied by Pulse Radiolysis, *J. Am. Chem. Soc.*, 2008, **130**, 14772-14777.

9. E. Balanikas, L. Martinez-Fernadez, R. Improta, P. Podbevsek, G. Baldacchino and D. Markovitsi, The Structural Duality of Nucleobases in Guanine Quadruplexes Controls Their Low-Energy Photoionization, *J. Phys. Chem. Lett.*, 2021, **12**, 8309−8313.